Int. J. Advanced Design and Manufacturing Technology, 2023, Vol. 16, No. 2, pp. 65-76

DOI: 10.30486/admt.2023.1967386.1378 ISSN: 2252-0406 https://admt.isfahan.iau.ir

Analysis of FGM Cylindrical Shell under Impact Loading of Explosion

Reza Azarafza[1, *]
Faculty of Materials and Manufacturing Technologies,
Malek Ashtar University of Technology, Tehran, Iran
E-mail: azarmut@mut.ac.ir
*Corresponding author

Pooya Pirali[2]
Faculty of Materials and Manufacturing Technologies,
Malek Ashtar University of Technology, Tehran, Iran
E-mail: ppirali@mut.ac.ir

Ali Javadi[3]
Faculty of Materials and Manufacturing Technologies,
Malek Ashtar University of Technology, Tehran, Iran
E-mail: javadiali22@gmail.com

Received: 9 September 2022, Revised: 27 January 2023, Accepted: 21 February 2023

Abstract: Due to the increasing application of Functionally Graded Materials (FGM) shells, it seems necessary to investigate their behaviour under different loads. Therefore, in this paper, the dynamic response of functionally graded materials cylindrical shells under explosive load has been investigated with analytical and simulation methods. LS-DYNA software is used in the simulation method. In analytical solution, vibration of composite circular cylindrical shells is investigated based on the first-order deformation shell theory. The boundary conditions are assumed to be fully simply supported. The dynamic response of composite shells is studied under blast loading. The modal technique is used to develop the analytical solution of composite shell. The solution for the shell under the giving loading condition can be found using the convolution integral. Material properties are assumed to be graded in the thickness direction according to Reddy function. A FGM cylindrical shell is made up of a mixture of ceramic and metal. Results show that the effect of explosion is such that it has the greatest effect on the inner layer and with increasing thickness to the outside of the shell this effect decreases and when the maximum deflection occurs, the dynamic velocity is zero. Also, it was observed that with increasing length, the radial deflection increases due to increasing the distance from the support to the center of the shell.

Keywords: Cylindrical Shell, Dynamic Loading**,** Explosion, FGM Shell

Biographical notes: Reza Azarafza received his Ph.D. in Mechanical Engineering from K. N. Toosi University of Technology (KNTU), Tehran, in 2005. His current research focuses on composite structures and Vibrations analysis. **Pooya Pirali** received his Ph.D. in Mechanical Engineering from Tarbiat Modares University in 2010. His current research focuses on plates and shell analysis. **Ali Javadi** received his M.Sc. in Mechanical Engineering from Malek Ashtar University of Technology in 2017, Tehran, Iran. His current research focuses on composite structures.

Research paper

1 INTRODUCTION

Functionally Graded Material (FGM) was first used as a thermal insulation in 1984 in a spacecraft project. Of course, before FGM, multilayer composites were used, but thermal stresses in these materials caused the delamination while this problem has been solved in FGM. FGMs are composite materials which are nonhomogeneous in microstructures, that mechanical properties change smoothly and continuously from one surface to another of the body. The most common type is a continuous combination of ceramic and metal. These materials are obtained by mixing metal and ceramic powder. The change of metal and ceramic from one surface to another is quite continuous, so that one surface is made of pure ceramic and the other surface is made of pure metal. Between the two levels is a continuous combination of both. In fact, the hardness of the metal and the high thermal resistance of the ceramic make it a widely used composite. One of the most widely used types of FGM is cylindrical shells. These shells, reinforced with beam-type elements, are widely used in mechanical structures such as missiles, submarines, rotary dryers, and aircraft fuel tanks. In most of these cases, the shell is under the dynamics and impact load due to the explosion, so it is necessary to study the behaviour of these structures under the explosion load [1].

Many works have been on the vibration and behaviour of cylindrical shells under dynamic and explosion load. Nosier performed a nonlinear analysis of a composite cylindrical shell. He used von Carmen nonlinear relations for strain-displacement relations and obtained the equilibrium Equations with the principle of minimum potential energy and first-order theory. jafari et al. [2] investigated the dynamic response of a composite cylindrical shell under radial impulse loading. They used two methods of numerical simulation and theoretical analysis. In this analysis, the first-order shear theory is used for equilibrium Equations and then, the Equations have been solved by Galerkin method. Dashtian et al. [3] investigated the fracture of grooved cylinders due to explosive loading caused by the explosion of the charge of HE. They numerically simulated the fracture time, fracture radius, fragmentation velocity, etc. using the explicit and nonlinear LS-Dina code. Azarafza et al. [4] investigated the response of a layered composite cylindrical shell under axial loading and lateral transient loading and obtained the effect of fiber angle, amount of load applied, internal pressure and some geometric parameters effecting on the shell response. Shukla et al. [5] performed their experiments on functional core composites. In this study, two types of cores with the same densities have been subjected to shock wave loading. Finally, the shock wave energy and the deformation energy of the sample were obtained based on the shock wave pressure profile and high-velocity deflection images. Haus et al. [6] investigated the explosion of functional material plates consisting of a metal-ceramic phase with a simple two-end support. In this research, the classical theory of plates is considered by considering the dynamic effects, damping effect and heat effects, and finally a dynamic and a static analysis based on the methods of Glerkin and Rang Kota have been presented. Aksoylar [7] performed nonlinear analysis of FGM and FML plates under explosive loading. In this research, the effect of volume fraction, load value and impulse function on the time response of the plate has been investigated. Kashani et al. [8] performed numerical analysis of the effect of the explosion of a cylindrical charge on armor made of functional material. In this research, Autodyne hydro code is used to simulate the explosion. Also, Kashani et al. [9] investigated the behaviour of the sic/steel functionally graded plate under the effect of the explosion of a cylindrical charge. In this study, Autodyne hydro code was used to simulate the explosion process and generate an explosion and shock wave. In order to achieve maximum efficiency based on the homogeneous bounded discrete layers method [10], they have made the plate consisting of eight separate layers, the initial and final layers of which are made of different material and the middle six layers are a combination of the two materials with different proportions. Darani et al. [11] simulated the explosion in cylindrical tanks using the JWL Equation. In order to model the behaviour of the cylinder material, they used the Johnson-Cook plasticity and fracture model. Also, the effect of explosive type, material and thickness of the cylinder on the fragmentation process of the cylinder and the velocity of the resulting fragments have been investigated and the simulation results have been compared with the experimental results.

In the past studies, little research has been done on the transient dynamic response of cylindrical shells of functionally graded materials based on the theory of first-order shear deformation under explosive impulse load inside the cylinder. So in this paper, the dynamic response of functionally graded materials cylindrical shells under explosive load have been done by analytical (based on the first-order deformation shell theory) and simulation method and the effect of different parameters on the dynamic response is investigated. The Boundary condition is simply supported (SS). Displacement components are the product of function of position and time. The function of position components of displacement was obtained in the form double Fourier series including of a modal beam functions in the axial direction and trigonometric functions in the tangential direction. In the analysis of transient dynamic response, the impulse load in the

form of triangular pulse was used to apply the dynamic charge of the explosion and the Jones-Wilkins-Lee (JWL) relationship was used to calculate the maximum pressure. The dynamic load of the explosion is applied as a function of time at the inner surface of the shell and function of time is obtained using the results of free vibration analysis and convolution integral. Then, the time response of the displacement components is derived using mode superposition method. To solve the governing Equations, a code was written using MATLAB software. Also, a simulation of shell with LS-DYNA software has been done. Since the FGM material model has not been defined in many explosion simulation software, the discrete layer theory was used in some part of the simulation. According to the results of this research and other studies, this assumption is acceptable and has enough accuracy and is currently one of the most reliable methods for simulating FGM materials. For the validation, the results of the analytical method (present) are compared with the simulation results and the reference results. Finally, the time response of displacements, stresses and dynamic velocities is derived. The effect of volume fractions, geometric parameters (such as thickness, radius, and length) on the radial displacement of the middle layer is investigated. Results show that the effect of explosion is such that it has the greatest effect on the inner layer and with increasing thickness to the outside of the shell this effect decreases and when the maximum deflection occurs, the dynamic velocity is zero. Also it was observed that with increasing length, the radial deflection increases due to increasing the distance from the support to the center of the shell.

2 GOVERNING EQUATIONS

Figure 1 shows a cylindrical shell with mean radius R, length L and thickness h.

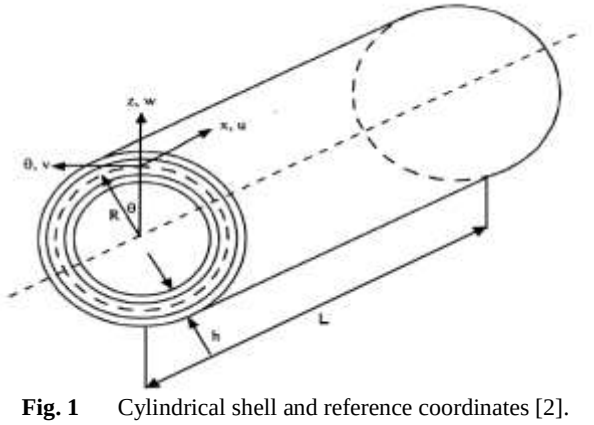

Fig. 1 Cylindrical shell and reference coordinates [2].

u, v and w are the displacement components in the axial (x), tangential (θ) and radial (z) direction respectively, and β_x ,the slopes in the plane are β_φ $x-z$ and $x-z$, respectively. According to the first-order shear deformation theory, equilibrium Equations are [2], [4]:

$$
\begin{aligned}
&R\frac{\partial N_x}{\partial x}+\frac{\partial N_{\varphi x}}{\partial \varphi}+Rq_x(x,\varphi,t)=R[I_1\frac{\partial^2 u}{\partial t^2}+I_2\frac{\partial^2 \beta_x}{\partial t^2}]\\
&\frac{\partial N_\varphi}{\partial \varphi}+R\frac{\partial N_{x\varphi}}{\partial x}-Q_\varphi+RN_x\frac{\partial^2 v}{\partial x^2}+Rq_\varphi(x,\varphi,t)=\\
&R[(I_1+\frac{2I_2}{R})\frac{\partial^2 v}{\partial t^2}+(I_2+\frac{I_3}{R})\frac{\partial^2 \beta_\varphi}{\partial t^2}]\\
&R\frac{\partial Q_x}{\partial x}+\frac{\partial Q_\varphi}{\partial \varphi}+N_\varphi+RN_x\frac{\partial^2 w}{\partial x^2}+Rq_z(x,\varphi,t)=RI_1\frac{\partial^2 w}{\partial t^2}\\
&R\frac{\partial M_x}{\partial x}+\frac{\partial M_{x\varphi}}{\partial \varphi}-RQ_x+Rm_x=R[I_2\frac{\partial^2 u}{\partial t^2}+I_3\frac{\partial^2 \beta_x}{\partial t^2}]\\
&\frac{\partial M_\varphi}{\partial \varphi}+R\frac{\partial M_{x\varphi}}{\partial x}-RQ_\varphi+Rm_\varphi=R[(I_2+\frac{2I_3}{R})\frac{\partial^2 v}{\partial t^2}+I_3\frac{\partial^2 \beta_\varphi}{\partial t^2}]
\end{aligned}
\tag{1}
$$

In the above relations, I_1, I_2 and I_3 are defined as follows:

$$(I_1,I_2,I_3)=\int_{-\frac{h}{2}}^{\frac{h}{2}}\rho_k(1,z,z^2)dz \tag{2}$$

ρ_k is density for each layer. The constitutive Equations of the FGM shells based on classical laminate theory are as follows:

$$
\begin{bmatrix} N_x\\ N_y\\ N_{xy}\\ M_x\\ N_y\\ M_{xy}\\ Q_x\\ Q_y \end{bmatrix}=\begin{bmatrix} A_{11} & A_{12} & 0 & B_{11} & B_{12} & 0 & 0 & 0\\ A_{21} & A_{22} & 0 & B_{21} & B_{22} & 0 & 0 & 0\\ 0 & 0 & A_{66} & 0 & 0 & B_{66} & 0 & 0\\ B_{11} & B_{12} & 0 & D_{11} & D_{12} & 0 & 0 & 0\\ B_{21} & B_{22} & 0 & D_{21} & D_{22} & 0 & 0 & 0\\ 0 & 0 & B_{11} & 0 & 0 & D_{66} & 0 & 0\\ 0 & 0 & 0 & 0 & 0 & 0 & H_{55} & H_{45}\\ 0 & 0 & 0 & 0 & 0 & 0 & H_{54} & H_{44} \end{bmatrix}\begin{bmatrix} \varepsilon_x^0\\ \varepsilon_\varphi^0\\ \gamma_{x\varphi}^0\\ k_x^0\\ k_\varphi^0\\ k_{x\varphi}^0\\ \gamma_{xz}^0\\ \gamma_{yz}^0 \end{bmatrix} \tag{3}
$$

Where A, B, D and H are the extensional, coupling, bending and thickness shear stiffness matrices, respectively, and are as follows:

$$\{A_{ij},B_{ij},D_{ij}\}=\int_{-\frac{h}{2}}^{\frac{h}{2}}\overline{Q_{ij}}(1,z,z^2)dz \tag{4}$$

$$\{H_{ij}\}=\int_{-\frac{h}{2}}^{\frac{h}{2}}k_0\overline{Q_{ij}}dz \tag{5}$$

Where, k_0 is the shear correction factor introduced by

Mindlin and is equal to $\frac{\pi^2}{12}$ [4]. $\overline{Q_{ij}}$ is the transformed reduced stiffness matrix [4]. The components of the strain field are defined as the first linear functions of the thickness coordinate according to the first approximation Love's theory] as follows [4]:

$$\begin{aligned}
\varepsilon_x &= \varepsilon_x^0 + zk_x^0 \\
\varepsilon_\varphi &= \varepsilon_\varphi^0 + zk_\varphi^0 \\
\varepsilon_{x\varphi} &= \gamma_{x\varphi}^0 + 2zk_{x\varphi}^0 \\
\varepsilon_{xz} &= \gamma_{xz}^0 \\
\varepsilon_{\varphi z} &= \gamma_{\varphi z}^0
\end{aligned} \tag{6}$$

Where, ε_x and ε_φ are the strains in the axial and tangential directions, respectively, and $\varepsilon_{x\varphi}$, ε_{xz} and $\varepsilon_{\varphi z}$ are the shear strains in the distance z from the middle surface and ε_x^0, ε_φ^0, $\gamma_{x\varphi}^0$, γ_{xz}^0 and $\gamma_{\varphi z}^0$ are the middle surface strains and k_x^0, k_φ^0 and $k_{x\varphi}^0$ are the curvatures and twist of the middle surface which are defined as follows:

$$\begin{Bmatrix} \varepsilon_x^0 \\ \varepsilon_\varphi^0 \\ \gamma_{x\varphi}^0 \end{Bmatrix} = \begin{Bmatrix} \dfrac{\partial u}{\partial x} \\ \dfrac{1}{R}\dfrac{\partial v}{\partial \varphi} + \dfrac{w}{R} \\ \dfrac{1}{R}\dfrac{\partial u}{\partial \varphi} + \dfrac{\partial v}{\partial x} \end{Bmatrix}, \begin{Bmatrix} k_x^0 \\ k_\varphi^0 \\ \varepsilon_{x\varphi}^0 \end{Bmatrix} = \begin{Bmatrix} \dfrac{\partial \beta_x}{\partial x} \\ \dfrac{1}{R}\dfrac{\partial \beta_\varphi}{\partial \varphi} \\ \dfrac{1}{R}\dfrac{\partial \beta_x}{\partial \varphi} + \dfrac{\partial \beta_\varphi}{\partial x} \end{Bmatrix} \tag{7}$$

$$\begin{Bmatrix} \gamma_{xz}^0 \\ \gamma_{\varphi z}^0 \end{Bmatrix} = \begin{Bmatrix} \beta_x + \dfrac{\partial w}{\partial x} \\ \beta_\varphi + \dfrac{1}{R}\dfrac{\partial w}{\partial \varphi} - \dfrac{v}{R} \end{Bmatrix}$$

3 SOLUTION METHOD

3.1. Boundary Conditions

The boundary conditions for the cylindrical shell which is simply supported along its curve edges at x = 0 and x = L are considered as:

$$N_x = M_x = w = v = \beta_\varphi = 0 \tag{8}$$

3.2. Free Vibration

With substituting the strain-displacement relations (Equation (7)) in Equation (3) and substituting them in Equilibrium Equations (1), the relations are summarized as follows:

$$[L]\{U\} = \{0\}$$

$$[L] = \begin{bmatrix} L_{11} & L_{12} & L_{13} & L_{14} & L_{15} \\ L_{21} & L_{22} & L_{23} & L_{24} & L_{25} \\ L_{31} & L_{32} & L_{33} & L_{34} & L_{35} \\ L_{41} & L_{42} & L_{43} & L_{44} & L_{45} \\ L_{51} & L_{52} & L_{53} & L_{54} & L_{55} \end{bmatrix} \quad \{U\} = \begin{Bmatrix} u(x,\varphi,t) \\ v(x,\varphi,t) \\ w(x,\varphi,t) \\ \beta_x(x,\varphi,t) \\ \beta_\varphi(x,\varphi,t) \end{Bmatrix} \tag{9}$$

L_{ij} are differential operators and are shown in Appendix A. In order to satisfy the boundary conditions, u, v, w, β_x and β_φ are defined as the following double Fourier series:

$$\begin{cases}
u = \sum_{m=1}^{\infty}\sum_{n=1}^{\infty} \overline{A_{mn}} T_{mn}(t) = \sum_{m=1}^{\infty}\sum_{n=0}^{\infty} A_{mn} \cos\dfrac{\lambda x}{l} \cos n\varphi T_{mn}(t) \\
v = \sum_{m=1}^{\infty}\sum_{n=1}^{\infty} \overline{B_{mn}} T_{mn}(t) = \sum_{m=1}^{\infty}\sum_{n=0}^{\infty} B_{mn} \sin\dfrac{\lambda x}{l} \sin n\varphi T_{mn}(t) \\
w = \sum_{m=1}^{\infty}\sum_{n=1}^{\infty} \overline{C_{mn}} T_{mn}(t) = \sum_{m=1}^{\infty}\sum_{n=0}^{\infty} C_{mn} \sin\dfrac{\lambda x}{l} \cos n\varphi T_{mn}(t) \\
\beta_x = \sum_{m=1}^{\infty}\sum_{n=1}^{\infty} \overline{D_{mn}} T_{mn}(t) = \sum_{m=1}^{\infty}\sum_{n=0}^{\infty} D_{mn} \cos\dfrac{\lambda x}{l} \cos n\varphi T_{mn}(t) \\
\beta_\varphi = \sum_{m=1}^{\infty}\sum_{n=1}^{\infty} \overline{E_{mn}} T_{mn}(t) = \sum_{m=1}^{\infty}\sum_{n=0}^{\infty} E_{mn} \sin\dfrac{\lambda x}{l} \sin n\varphi T_{mn}(t)
\end{cases} \tag{10}$$

A_{mn}, B_{mn}, C_{mn}, D_{mn} and E_{mn} are constant coefficients of the natural mode associated with the free vibration problems, *m* is the axial half wav number and *n* is the circumferential wave number and $T_{mn}(t)$ is the time function of displacement and slop. To solve the free vibration analysis, function of time is treated as $T_{mn}(t) = e^{i\omega_{mn}t}$, where ω_{mn} is the natural frequency.

By substituting the relations of the displacement components 10 in relation 9 and by sorting, the following relation is obtained:

$$\begin{bmatrix} C_{11} & C_{12} & C_{13} & C_{14} & C_{15} \\ C_{21} & C_{22} & C_{23} & C_{24} & C_{25} \\ C_{31} & C_{32} & C_{33} & C_{34} & C_{35} \\ C_{41} & C_{42} & C_{43} & C_{44} & C_{45} \\ C_{51} & C_{52} & C_{53} & C_{54} & C_{55} \end{bmatrix} \begin{Bmatrix} A_{mn} \\ B_{mn} \\ C_{mn} \\ D_{mn} \\ E_{mn} \end{Bmatrix} = 0 \tag{11}$$

That components of C_{ij} are shown in the appendix B. By setting determinant of coefficients equal to zero, the characteristic frequency Equation is obtained.

$$\beta_1\omega^{10} + \beta_2\omega^8 + \beta_3\omega^6 + \beta_4\omega^4 + \beta_5\omega^2 = 0 \tag{12}$$

Where, β_i are constant coefficients. By solving this Equation (12), the natural frequencies are obtained and by substituting these frequencies in Equation (11), the constant coefficients of mode shape of the modes are obtained.

3.3. Dynamic Response Analysis Under Impulse Load

The applied load is assumed to be only in the radial direction and there is no external excitation in the other directions. For the simple support, results are obtained as follows [12]:

$$q_z(x,\varphi,t) = Q_z(x,\varphi)\, f(t) = \sum_{m=1}^{\infty}\sum_{n=0}^{\infty} P_{mn} \sin\frac{\lambda x}{l}\cos n\varphi\, f(t) \tag{13}$$

Where, P_{mn} is a constant coefficient that can be calculated from the profile of the applied load and $f(t)$ is a function of time. So, to calculate the coefficient P_{mn}, the sides of Equation (13), are multiplied by $\sin\frac{m\pi x}{L}\cos n\varphi$ and integrate it as a result:

$$\begin{aligned} n=0,\quad & P_{m0} = \frac{2}{\pi L}\int_0^L\int_{-\pi}^{\pi} q_z(x,\varphi)\sin\frac{m\pi x}{l}\, dx d\varphi \\ n>0,\quad & P_{mn} = \frac{2}{\pi L}\int_0^L\int_{-\pi}^{\pi} q_z(x,\varphi)\sin\frac{m\pi x}{l}\cos n\varphi\, dx d\varphi \end{aligned} \tag{14}$$

Which the maximum explosion pressure obtained from the JWL Equation [13] is in the above relation is.

$$P = A\left(1-\frac{\omega\rho}{R_1\rho_0}\right)e^{-R_1\frac{\rho_0}{\rho}} + B\left(1-\frac{\omega\rho}{R_2\rho_0}\right)e^{-R_1\frac{\rho_0}{\rho}} + \frac{\omega\rho^2}{\rho_0}E_m \tag{5}$$

Where, P is the pressure, A, B, R_1, R_2, and ω are constants of the explosive, ρ_0, is the density of the explosive, ρ is the density of the explosive products and E_m, internal energy is an explosive per unit mas given in the "Table 1".

Table 1 Constants of JWL Equation [13]

Material properties	A (Mpa)	B (Mpa)	R_1	R_2	ω
TNT	373770	3747.1	4.15	0.9	0.35
P (Mpa)	V (m/ms)	Em (MJ/m^3)	ρ_0 (kg/m^3)		
21000	6.93	0.08	16300		

By substituting the assumed displacement of Equation (10) in Equilibrium Equations (1) and using the results of free vibrations, the following Equations are obtained:

$$\begin{aligned} & -w_{mn}^2 T_{mn}(t)[I_1\overline{A_{mn}} + I_2\overline{D_{mn}}] = \ddot{T}_{mn}(t)[I_1\overline{A_{mn}} + I_2\overline{D_{mn}}] \\ & -w_{mn}^2 T_{mn}(t)[(I_1+\frac{2I_2}{R})\overline{B_{mn}} + (I_2+\frac{I_3}{R})\overline{E_{mn}}] = \\ & \ddot{T}_{mn}(t)[(I_1+\frac{2I_2}{R})\overline{B_{mn}} + (I_2+\frac{I_3}{R})\overline{E_{mn}}] \\ & -w_{mn}^2 T_{mn}(t) I_1\overline{C_{mn}} = \ddot{T}_{mn}(t) I_1\overline{C_{mn}} - q_z(x,\varphi,t) \\ & -w_{mn}^2 T_{mn}(t)[I_2\overline{A_{mn}} + I_3\overline{D_{mn}}] = \\ & \ddot{T}_{mn}(t)[I_2\overline{A_{mn}} + I_3\overline{D_{mn}}] \\ & -w_{mn}^2 T_{mn}(t)[(I_2+\frac{2I_3}{R})\overline{B_{mn}} + I_3\overline{E_{mn}}] = \\ & \ddot{T}_{mn}(t)[(I_1+\frac{2I_2}{R})\overline{B_{mn}} + I_3\overline{E_{mn}}] \end{aligned} \tag{16}$$

After summation of two sides of the above Equations and simplifying a second-order differential Equation in terms of time, the result is as follows:

$$\ddot{T}_{mn}(t) + w_{mn}^2 T_{mn}(t) = G_{mn}(t) \tag{17}$$

Where, $G_{mn}(t)$ is the generalized force and is:

$$G_{mn}(t) = \frac{1}{J_{mn}}\int_0^L\int_0^{2\pi} f_r(x,\theta,t) C_{mn}\, dx d\theta \tag{18}$$

The J_{mn} is the normalized mass and is obtained as follows:

$$\begin{aligned} J_{mn} = {} & I_1(A_{mn}^2 + B_{mn}^2 + C_{mn}^2) + 2I_2(A_{mn}D_{mn} + B_{mn}E_{mn} + \frac{1}{R}B_{mn}^2) \\ & + I_3(D_{mn}^2 + E_{mn}^2 + \frac{2}{R}B_{mn}E_{mn}) \end{aligned} \tag{19}$$

By substituting Equations (18) and (13) in Equation (17) and some simplification, the following relation is obtained:

$$\ddot{T}_{mn}(t) + \omega_{mn}^2 T_{mn}(t) = \frac{P_{mn}(t) C_{mn}(t) F(t)}{N_{mn}} \tag{20}$$

Where, N_{mn} is equal to:

$$\begin{aligned} N_{mn} = {} & I_1(A_{mn}^2 + B_{mn}^2 + C_{mn}^2) + 2I_2(A_{mn}D_{mn} + B_{mn}E_{mn} + \frac{1}{R}B_{mn}^2) + \\ & I_3(D_{mn}^2 + E_{mn}^2 + \frac{2}{R}B_{mn}E_{mn}) \end{aligned} \tag{21}$$

Using the Laplace transform, the solution of Equation 20 for the zero initial conditions is as follows:

$$T_{mn}(t)=\frac{P_{mn}C_{mn}}{N_{mn}\omega_{mn}}\int_0^t f(\tau)\sin\omega_{mn}(t-\tau)d\tau \qquad (22)$$

Finally, the time response of the FGM cylindrical shell with simply supported boundary conditions under the impulse of the blast load based on mode superposition theory is obtained as follows:

$$\begin{aligned}
u&=\sum_{m=1}^{\infty}\sum_{n=1}^{\infty}\frac{P_{mn}C_{mn}}{J_{mn}\omega_{mn}}A_{mn}\cos\frac{m\pi x}{L}\cos n\varphi\int_0^t f(\tau)\sin\omega_{mn}(t-\tau)d\tau\\
v&=\sum_{m=1}^{\infty}\sum_{n=1}^{\infty}\frac{P_{mn}C_{mn}}{J_{mn}\omega_{mn}}B_{mn}\sin\frac{m\pi x}{L}\sin n\varphi\int_0^t f(\tau)\sin\omega_{mn}(t-\tau)d\tau\\
w&=\sum_{m=1}^{\infty}\sum_{n=1}^{\infty}\frac{P_{mn}C_{mn}^{2}}{J_{mn}\omega_{mn}}\sin\frac{m\pi x}{L}\cos n\varphi\int_0^t f(\tau)\sin\omega_{mn}(t-\tau)d\tau\\
\beta_x&=\sum_{m=1}^{\infty}\sum_{n=1}^{\infty}\frac{P_{mn}C_{mn}}{J_{mn}\omega_{mn}}D_{mn}\cos\frac{m\pi x}{L}\cos n\varphi\int_0^t f(\tau)\sin\omega_{mn}(t-\tau)d\tau\\
\beta_\varphi&=\sum_{m=1}^{\infty}\sum_{n=1}^{\infty}\frac{P_{mn}C_{mn}}{J_{mn}\omega_{mn}}E_{mn}\sin\frac{m\pi x}{L}\sin n\varphi\int_0^t f(\tau)\sin\omega_{mn}(t-\tau)d\tau
\end{aligned} \qquad (23)$$

It should to be noted that the mode shape coefficients (A_{mn}, B_{mn},C_{mn},D_{mn} and E_{mn}) are calculated by the use of Equation (14) together with the property of mode shape orthogonality with response to mass matrix. As shown in Equations (23), the shell displacement response consists of function of position and time. The position function of the response is the mode shape (derived from free vibrations) and its time function is the convolution integral, which must be calculated according to the type of pulse. The triangular pulse shown in "Fig. 2". The convolutional integral for this pulse is calculated as follows:

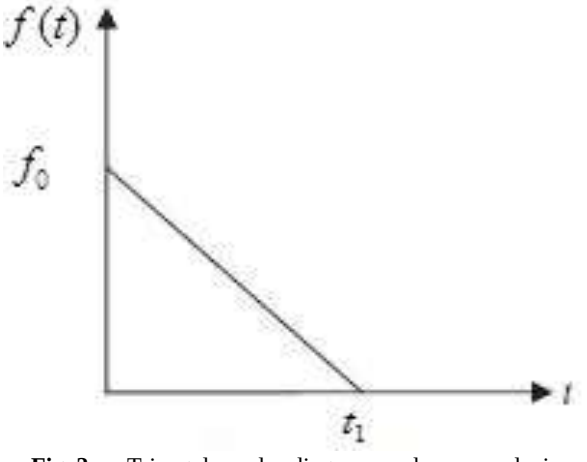

Fig. 2 Triangular pulse diagram used as an explosive pulse [2].

$$\begin{cases} f(t)=f_0(1-\dfrac{t}{t_1}) & 0\le t\le t_1\\ f(t)=0 & t>t_1 \end{cases}$$

$$\int_0^t f(\tau)\sin\omega_{mn}(t-\tau)d\tau=$$

$$\begin{cases} \dfrac{f_0}{\omega_{mn}}[1-\cos\omega_{mn}t+\dfrac{\sin\omega_{mn}t}{\omega_{mn}t_1}-\dfrac{t}{t_1}] & 0\le t\le t_1\\ f_0[\dfrac{-1}{\omega_{mn}}\cos\omega_{mn}t+\dfrac{2\cos\omega_{mn}(t-t_1)\sin\omega_{mn}\frac{t_1}{2}}{\omega_{mn}^2t_1}] & t>t_1 \end{cases} \qquad (24)$$

The above relationship f_0 is the maximum pressure that is applied. Now, with determined time function, P_{mn} shapes and normalized mode ω_{mn} ,J_{mn} , dynamic displacements E_{mn} and A_{mn}, B_{mn},C_{mn},D_{mn} can be obtained and strains can be found through them and then, stresses can be obtained through strains. To obtain the numerical result, a computer code was written.

4 RESULTS AND DISSCUSIONS

In order to ensure the accuracy of the obtained results, the time response (maximum radial displacement) of the present method was compared with Ref. [2] in "Fig. 3". "Table 2" shows the geometric properties of composite. It can be seen that good agreement is obtained between the results.

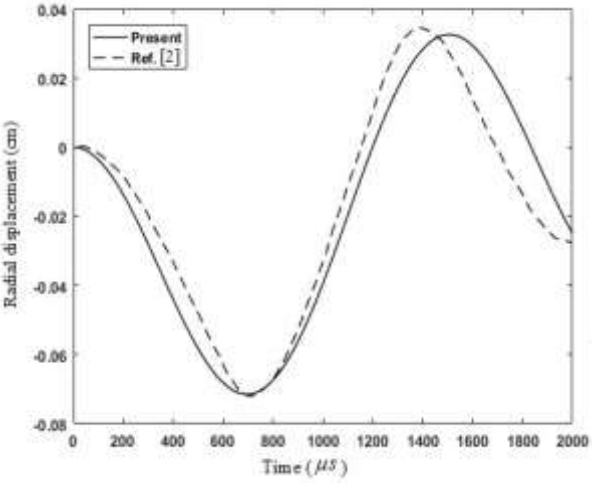

Fig. 3 Comparison of the central deflection of simply supported composite cylindrical shell with Ref.[2].

Table 2 Geometrical properties of composite

Radius (cm)	Length (cm)	Thickness (cm)	*m*	*n*
20	20	0.12	27	35

The percentage error of the two methods is shown in "Table 3". As can be seen, the maximum deflection occurs at about the same time and the percentage error is about 1.11%.

Table 3 Maximum deflection and its occurrence time for the present study and Ref. [2]

	Max. Deflection (cm)	Max. Deflection time (μs)
Ref. [2]	0.0718	707
Present Study	0.071	694
Error (%)	1.11	

So to confirm the results, a simulation with LS-DYNA software was performed and then the results were compared for an FGM cylindrical shell. "Tables 4 and 5" show the geometric and mechanical properties of FGM cylindrical shell, respectively.

Table 4 Dimensions of the shell

Thickness (cm)	Length (cm)	Radius (cm)
1	80	40

Table 5 Mechanical Properties of FGM shell [9].

Material rpoperties	Sic	Al
Density (gr/cm^3)	3.16	2.78
Young's Modulus (Mbar)	4.23	0.731
Tangential Shear Modulus (Mbar)	0.28	1.83
Poisson's Ratio	0.16	0.31

Figure 4 shows the time response of analytical method and simulation with LS-DYNA. These results have good agreements with LS-DYNA.

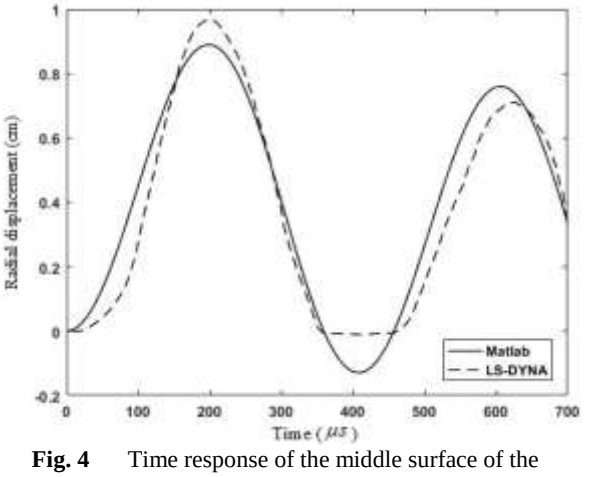

Fig. 4 Time response of the middle surface of the simulation and analytical method.

Figure 5 shows the deflection of middle surface in the longitudinal direction. As can be seen, the maximum radial rise occurs in the middle of the shell (x = 40) and the zero at the supports (x = 0, x = 80). The maximum values for analysis and simulation are given in "Table 6". "Table 6" shows that the maximum radial deflection and the time of its occurrence in both methods have good agreement and have a difference of 8.2%. Finally, according to the longitudinal diagram and also the comparisons between two methods, the accuracy of the results can be ensured.

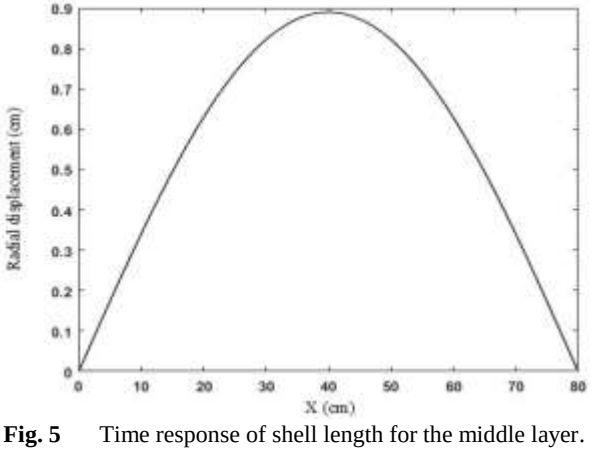

Fig. 5 Time response of shell length for the middle layer.

Table 6 Maximum radial deflection and time of its occurrence

Solving Method	Analytical Method	Numerical Method
Deflection (w) (cm)	0.8892	0.9684
Time (μs)	199.574	201.953
Discrepancy (%)	8.2	

4.1. Displacements

In the following, all diagrams are drawn for the geometric properties of "Table 4" and the mechanical properties of "Table 5". In all cases, the volume fraction of zero indicates a complete ceramic and a volume fraction of 1 complete metal. The explosive is TNT with a mass of 4 kilograms, which is placed right in the center of the shell. Analysis time is 700 μs .

Figure 6 shows the effect of volume fraction on the time response of displacement and slop for center point of FGM cylindrical shell over time. Results show that the displacement of the circumferential and Longitudinal, β_x and β_y increased with decreasing of volume fraction. So that the minimum deflection and slope occurs at the highest volume fraction. Thus, with two, three and five times the volume fraction, the deflection of circumferential, Longitudinal, slop of β_x and β_y decrease to 4.41%, 8.6% and 16%, respectively.

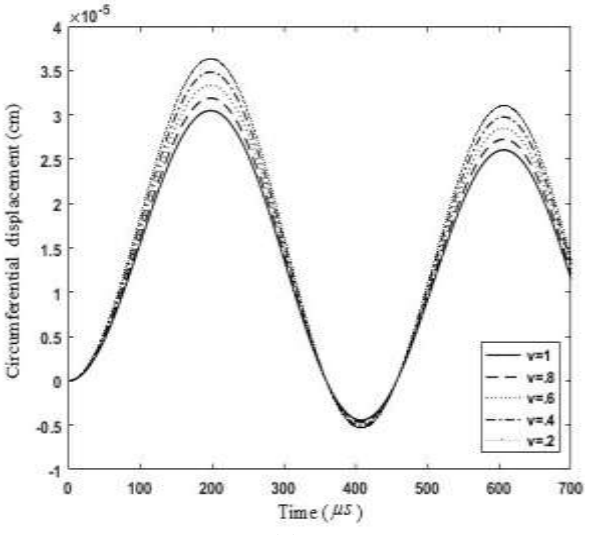

(a)

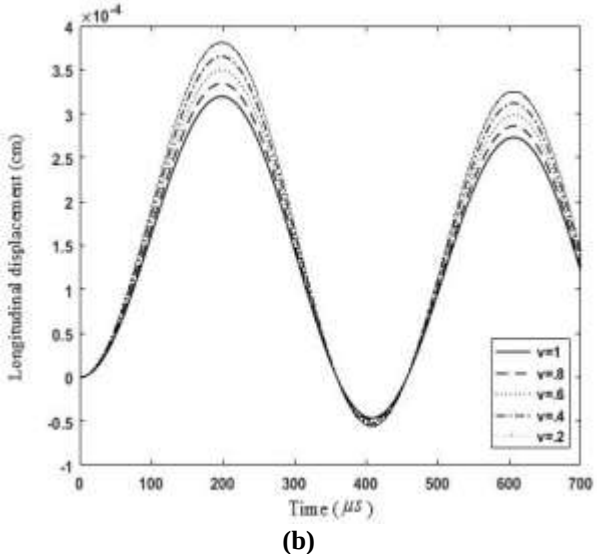

(b)

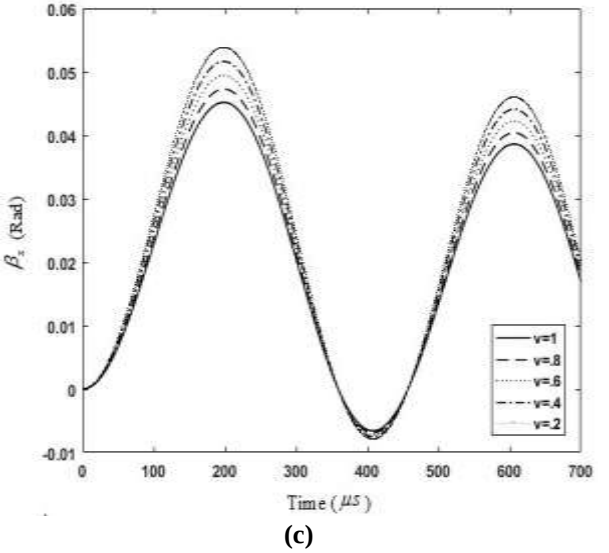

(c)

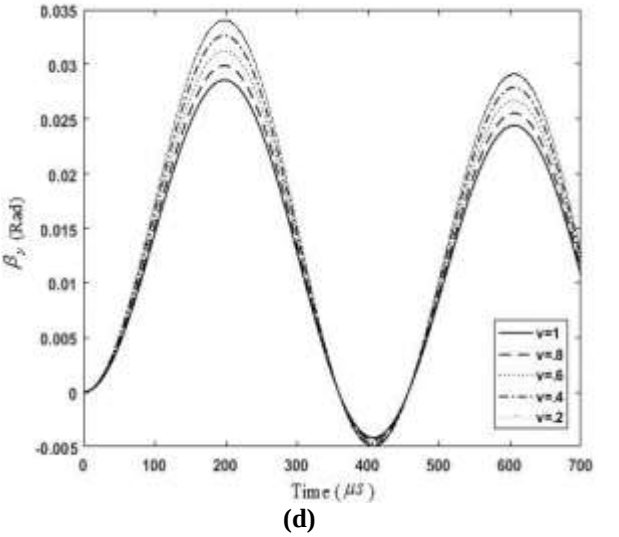

(d)

Fig. 6 Time response of center point of FGM cylindrical shell under different volume fraction: (a): tangential displacement, (b): longitudinal displacement, (c): slop β_x, and (d): slop β_y.

Figure 7 shows the effect of volume fraction on the displacement of the circumferential and longitudinal, β_x and β_y along with the length of shell for center point of FGM cylindrical shell. As can be seen, displacement and slope decreased with increasing of volume fraction. In "Figs. 7a and 7c", in the middle of the length of the cylinder (x=40), the displacement and slop are zero and the maximum displacement and slop occurs at both ends of the shell. Also, in "Figs. 7b and 7d", in the middle of the length of the shell (x=40), the displacement and slop are maximum and at both ends of the shell are zero.

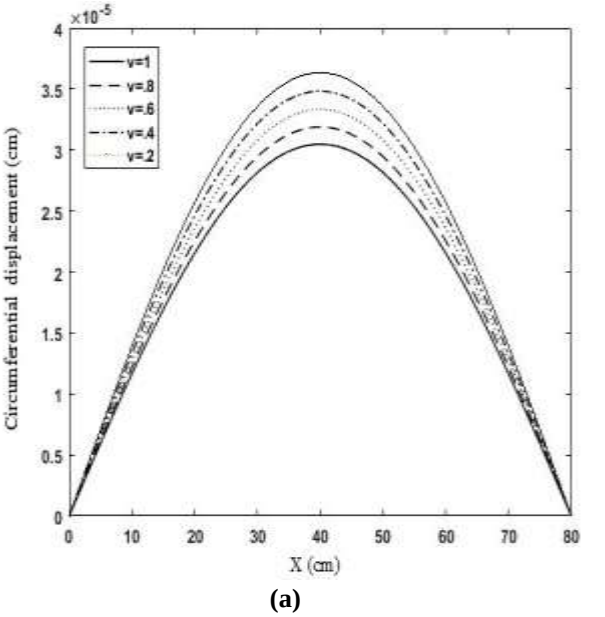

(a)

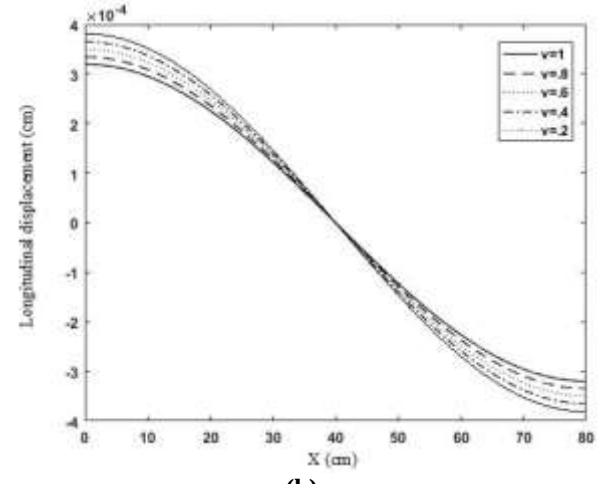

(b)

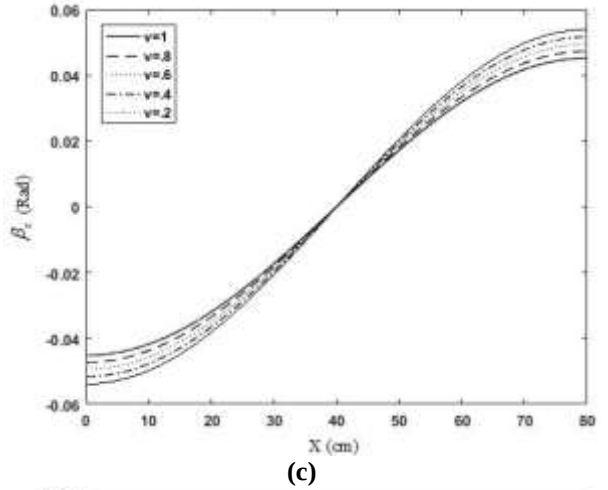

(c)

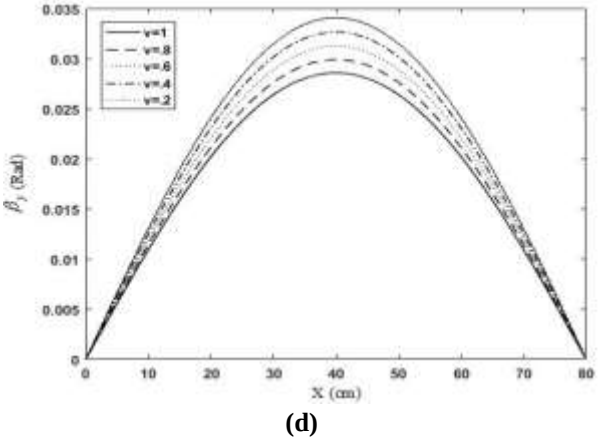

(d)

Fig. 7 Effect of volume fraction on the center point of FGM cylindrical shell: (a): tangential displacement, (b): longitudinal displacement, (c): slop β_x, and (d): slop β_y.

4.2. Strains

Figure 8 shows the variation of time response of center point of cylindrical shell with volume fraction. It is observed that in all cases, the lowest strain occurs at the highest volume fraction. As the volume fraction increases, the shell strength increases, so less deflection occurs and consequently less strain occurs.

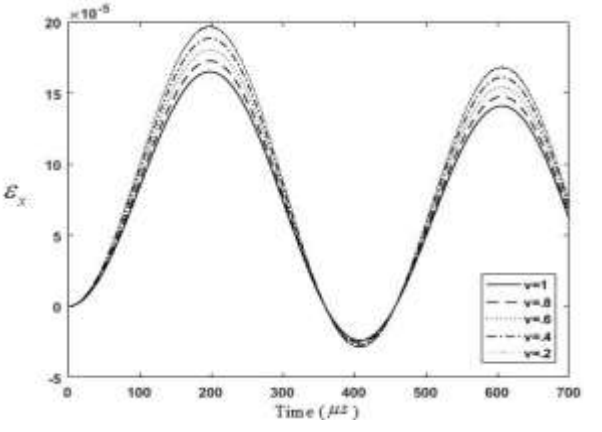

(a)

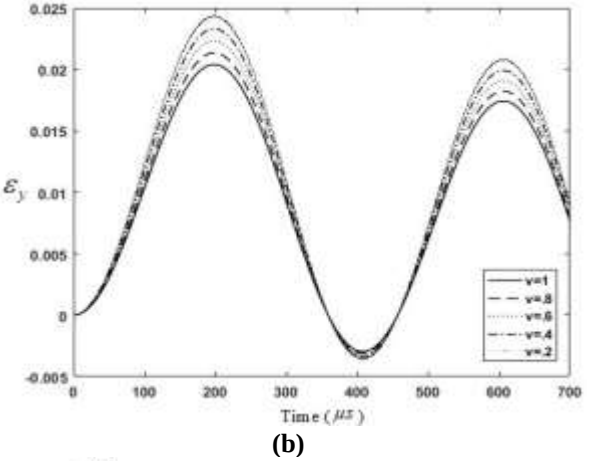

(b)

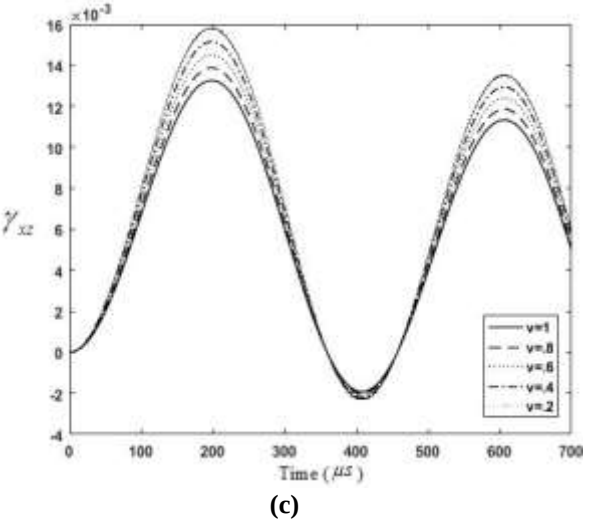

(c)

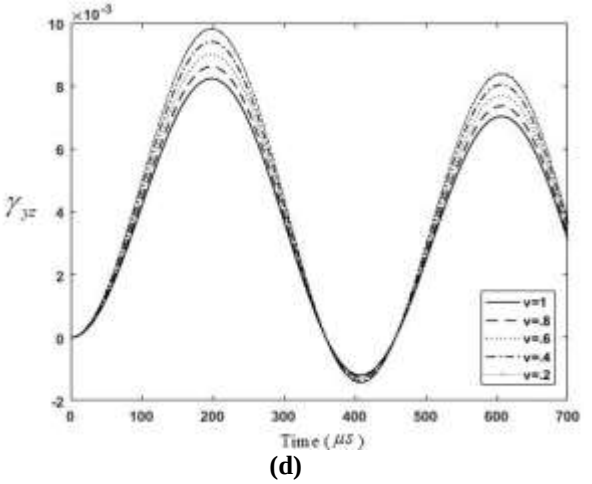

(d)

Fig. 8 Variation of time response of center point of cylindrical shell with volume fraction: (a): ε_x, (b): ε_y, (c): γ_{xz}, and (d): γ_{yz}.

4.3. Dynamic Velocity in Radial Direction

Figure 9 shows the effect of volume fraction on the dynamic velocity in radial directions for center point of FGM cylindrical shell.

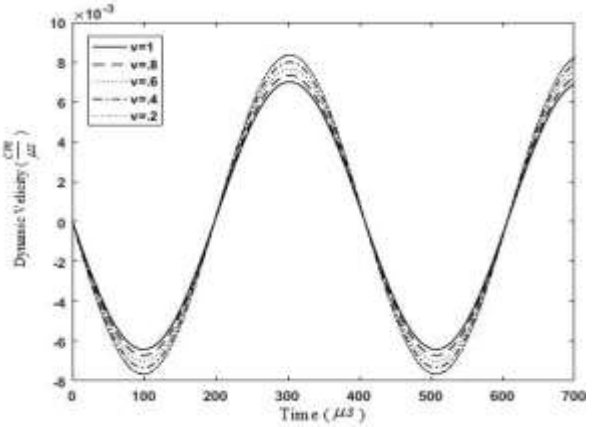

(a)

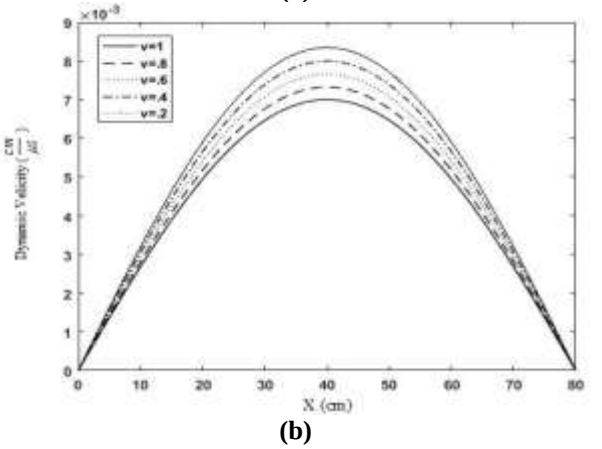

(b)

Fig. 9 Effect of volume fraction on the dynamic velocity in radial directions for center point of FGM cylindrical shell.

It can be seen that with decreasing volume fraction, the maximum dynamic velocity increases. According to the "Fig. 9b", maximum dynamic velocity occurs in the middle of the shell, because the middle of the shell is the farthest distance from the supports.

4.4. The Effect of Geometric Parameters and Mass of The Explosive on The Radial Displacement of The Middle Layer

"Table 7" shows the effect of increasing the shell thickness on the maximum deflection.

Table 7 Effect of increasing the t/R of the shell on the deflection of the shell

t/R	Max. Radial Deflection (cm)	Time (μs)	Longitudinal direction (cm)
0.0125	1.771	199.574	40
0.025	0.8893	199.574	40
0.0375	0.5934	199.574	40
0.05	0.4385	199.574	40
0.0625	0.3795	199.574	40
0.0725	0.3011	199.574	40
0.0875	0.2560	199.574	40
0.1	0.2273	199.574	40

Results show that with increasing t/R, the maximum radial deflection decreases, so that by increasing the shell thickness as twice, it deflection is about halved. "Table 8" shows the effect of increasing the L/R on radial deflection.

Table 8 Maximum radial deflection for different shell lengths

Shell Length (cm)	L/R	Max. Radial Deflection (cm)
80	2	0.8893
160	4	1.773

As can be seen, with increasing the L/R, the radial deflection increases so that by doubling, this ratio has almost doubled. "Table 9" shows the effect of increasing the mass of explosives on radial deflection.

Table 9 Maximum radial deflection for different TNT masses

TNT mass (kg)	1	2	3	4	5	6	7
Max. Radial Deflection (cm)	0.07	0.26	0.53	0.89	1.32	1.81	2.32

The results show that with increasing mass of explosives, the radial deflection increases. By multiplying the mass of the explosive by 7 times, the maximum deflection increases by 33 times.

5 CONCLUSIONS

In the present study, the transient dynamic response of FGM cylindrical shells under explosive load has been investigated based on the first-order shear deformation theory. The Boundary condition is simply supported (SS). Displacement components are the product of function of position and time. The function of position components of displacement was obtained in the form of double Fourier series including a modal beam functions in the axial direction and trigonometric functions in the tangential direction. In the analysis of transient dynamic response, the impulse load in the form of triangular pulse was used to apply the dynamic charge of the explosion and the Jones-Wilkins-Lee (JWL) relationship was used to calculate the maximum pressure. Also, a simulation of shell with LS-DYNA software has been done. Finally, the effect of volume fractions on the time response of displacements and dynamic velocities is derived and the following results have been obtained:

1- The effect of explosion on different volumetric fractions of the shell is such that it has the greatest effect on the inner layer and with increasing thickness to the outside of the shell (increasing the volume fraction of metal), this effect decreases. So that in most of the volumetric fractions studied, a very small difference can be observed between two consecutive volume fractions. These results include displacements, stresses, and strains.

2. The dynamic velocity diagram of the middle layer has a sinusoidal shape. When the maximum deflection occurs, the dynamic velocity is zero, and at the turning points of the chart, the dynamic velocity reaches its maximum value.

3- To observe the effect of shell thickness on its response, the shell was examined in eight different thicknesses. Comparisons show that with increasing thickness, the amount of deflection decreases

4- By examining the effect of changing the length and radius of the shell, it was observed that with increasing length, the radial deflection increases due to increasing the distance from the support to the center of the shell. Also, as the radius decreases, the radial deflection increases.

5- As the mass of the explosive increases, its explosive pressure increases leading to deflection increases, so that by multiplying the mass of the explosive by 7 times, the maximum has increased by 33 times.

6- Also in N = 0 (ceramic), there is the lowest deflection and with increasing the amount of N (increasing the volume fraction of metal), the deflection increscent is more.

APPENDIX A

$$L_{11} = [(A_{11}R)\frac{\partial^2}{\partial x^2} + (\frac{A_{66}}{R})\frac{\partial^2}{\partial \varphi^2}]$$

$$L_{12} = L_{21} = [(A_{12} + A_{66})\frac{\partial^2}{\partial x\,\partial \varphi}]$$

$$L_{13} = -L_{31} = [(A_{12})\frac{\partial}{\partial x}]$$

$$l_{14} = l_{41} = [(B_{11}R)\frac{\partial^2}{\partial x^2} + (\frac{B_{66}}{R})\frac{\partial^2}{\partial \varphi^2}]$$

$$L_{15} = L_{51} = [(B_{12} + B_{66})\frac{\partial^2}{\partial x\,\partial \varphi}]$$

$$L_{22} = [(A_{66}R)\frac{\partial^2}{\partial x^2} + (\frac{A_{22}}{R})\frac{\partial^2}{\partial \varphi^2} - \frac{H_{44}}{R}]$$

$$L_{23} = -L_{32} = [(H_{45})\frac{\partial}{\partial x} + (\frac{A_{22} + H_{44}}{R})\frac{\partial}{\partial \varphi}]$$

$$L_{24} = L_{42} = [(B_{12} + B_{66})\frac{\partial^2}{\partial x\,\partial \varphi} + H_{45}]$$

$$L_{25} = L_{52} = [(B_{66}R)\frac{\partial^2}{\partial x^2} + (\frac{B_{22}}{R})\frac{\partial^2}{\partial \varphi^2} + H_{44}]$$

$$L_{33} = [(H_{55}R)\frac{\partial^2}{\partial x^2} + (2H_{45})\frac{\partial^2}{\partial x\,\partial \varphi} + (\frac{H_{44}}{R})\frac{\partial^2}{\partial \varphi^2} - \frac{A_{22}}{R}]$$

$$L_{34} = L_{43} = [(H_{55}R - B_{12})\frac{\partial}{\partial x} + (H_{45})\frac{\partial}{\partial x}]$$

$$L_{35} = -L_{53} = [(H_{45}R)\frac{\partial}{\partial x} + (H_{44} - \frac{B_{22}}{R})\frac{\partial}{\partial \varphi}]$$

$$L_{44} = [(D_{11}R)\frac{\partial^2}{\partial x^2} + (\frac{D_{66}}{R})\frac{\partial^2}{\partial \varphi^2} - (H_{55})R]$$

$$L_{45} = L_{54} = [(D_{12} + D_{66})\frac{\partial^2}{\partial x\,\partial \varphi} - H_{45}R]$$

$$L_{55} = [(D_{66}R)\frac{\partial^2}{\partial x^2} + (\frac{D_{22}}{R})\frac{\partial^2}{\partial \varphi^2} - H_{44}R]$$

APPENDIX B

C_{ij}

$c_{11} = k_{11} - \omega^2 M_{11}$, $c_{12} = k_{12}$, $c_{13} = k_{13}$,

$c_{14} = k_{14} - \omega^2 M_{14}$, $c_{15} = k_{15}$

$c_{21} = k_{21}$, $c_{22} = k_{22} - \omega^2 M_{22}$, $c_{23} = k_{23}$,

$c_{24} = k_{24}$, $c_{25} = k_{25} - \omega^2 M_{22}$

$c_{31} = k_{31}$, $c_{32} = k_{32}$, $c_{33} = k_{33} - \omega^2 M_{33}$,

$c_{34} = k_{34}$, $c_{35} = k_{35}$

$c_{41} = k_{41} - \omega^2 M_{41}$, $c_{42} = k_{42}$, $c_{43} = k_{43}$,

$c_{44} = k_{44} - \omega^2 M_{44}$, $c_{45} = k_{45}$

$c_{51} = k_{51}$, $c_{52} = k_{52} - \omega^2 M_{52}$, $c_{53} = k_{53}$,

$c_{54} = k_{54}$, $c_{55} = k_{55} - \omega^2 M_{52}$

REFERENCES

[1] Nosier, A., Reddy, J. N., Study of Non-Linear Dynamic Equations of Higher-Order Shear Deformation Plate Theories, International Journal of Non-Linear Mechanics, Vol. 26, No. 2, 1991, pp. 233-249, Doi.org/10.1016/0020-7462(91)90054-W.

[2] Jafari, A. A., Khalili, S.M.R., and Azarafza, R., Transient Dynamic Response of Composite Circular Cylindrical Shells Under Radial Impulse Load and Axial Compressive Loads, Thin-Walled Structures, Vol. 43, 2005, pp. 1763-1786, DOI:10.1016/j.tws.2005.06.009.

[3] Dashtian Gerami, N., Khodarahmi, H., and Khazraeian, N., Fracture of Cylindrical Grooves in The Middle of a Groove Due to Cost Explosion, 13th Annual Conference on Mechanical Engineering, Isfahan, Isfahan University of Technology, 2005 (In Persian).

[4] Azarafza, R., Khalili, S. M. R., Jafari, A. A., and Davar, A., Analysis and Optimization of Laminated Composite Circular Cylindrical Shell Subjected to Compressive Axial and Transverse Transient Dynamic Loads, Thin-Walled Structures, Vol. 47, 2005, PP. 970-983, DOI: 10.1016/j.tws.2009.01.004.

[5] Wange, E., Gardner, N., and Shukla, A., The Blast Resistance of Sandwich Composites with Stepwise Graded Cores, International Journal of Solids and Structures, Vol. 46, 2009, No. 18-19, pp. 3492-3502, DOI.org/10.1016/j.ijsolstr.2009.06.004.

[6] Hause, T., Advanced Functionally Graded Plate-Type Structures Impacted by Blast Loading, International Journal of Impact Engineering, Vol. 38, No. 5, 2011, pp. 314-321, DOI.org/10.1016/j.ijimpeng.2010.11.006.

[7] Aksoylar, C., Omercikoglu, A., Mecitoglu, Z., and Omurtag, M. H., Nonlinear Transient Analysis of FGM and FML Plate Under Blast Loads by Experimental and Mixed FE Methods, Composite structure, Vol. 94, No. 2, 2012, pp. 731–744, DOI.org/10.1016/j.compstruct.2011.09.008.

[8] Kashani, M., Peyman, S., Numerical Analysis of the Explosion Effect of a Cylindrical Charge on Armor Made of Functional Material (Aluminum Nitride- Aluminum), 8th National Congress of Civil Engineering, Faculty of Civil Engineering, Babol, May, 2014, (In Persian), COI: AEBSCONF02_188.

[9] Kashani, M., Peyman, S., Investigation of Functional Plate Behavior (Silinium-Steel) under the Explosion of Cylindrical Explosion Pressure", 8th National Congress of Civil Engineering, Faculty of Civil Engineering, Babol, May, 2014, (In Persian).

[10] Banks-Sills, L., Eliasi, R., and Berlin Y., Modeling of Functionally Graded Material in Dynamic Analysis, Composites Part B: Engineering, Vol. 33, No. 1, 2002, pp. 7-15, 2002, DOI.org/10.1016/S1359-8368(01)00057-9.

[11] Mahmoudi Darani, S., and Aghagol, A., Numerical Simulation of Explosions in Cylindrical Tanks Using Euler-Lagrange Simultaneous Technique, 12th National Conference on Manufacturing Engineering of Iran, Tehran, Iranian Society of Manufacturing Engineering, Tehran, Faculty of Engineering, 2011, (In Persian).

[12] Azarafza, R., Weight and Dynamic Optimization of Multilayer Composite Cylindrical Structures, Ph.D. Dissertation, Mechanical Engineering Dept., K.N.T. University, September, 2005.

[13] Taghavi Parsa, M. H., Peyman, S., Analysis of the Effect of Buried Explosive Loading on Underground Reinforced Concrete Structures, Amirkabir Journal of Civil Engineering, Vol. 51, No. 1, 2019, pp. 3-18, DOI: 10.22060/ceej.2018.12858.5288.